

Inertial control of the mirror suspensions of the VIRGO interferometer for gravitational wave detection.*

G.Losurdo[†], G.Calamai¹, E.Cuoco¹, L.Fabbroni,
G.Guidi², M.Mazzoni¹, R.Stanga¹, F.Vetrano²

Istituto Nazionale di Fisica Nucleare - Sezione di Firenze

¹*also: Università degli Studi di Firenze*

²*also: Università degli Studi di Urbino*

L.Holloway[‡]

University of Illinois, Urbana, IL

D.Passuello, G.Ballardin, S.Braccini, C.Bradaschia, R.Cavaliere, R.Cecchi, G.Cella³,
V.Dattilo, A.Di Virgilio, F.Fidecaro³, F.Frasconi, A.Gennai[§], A.Giazotto, I.Ferrante,
P.La Penna, F.Lelli, T.Lomtadze, A.Marin^{**}, S.Mancini, F.Paoletti, A.Pasqualetti,
R.Passaquieti³, R.Poggiani³, R.Taddei, A.Vicerè^{††}, Z.Zhang

Istituto di Fisica Nucleare - Sez. di Pisa

³*also: Università degli Studi di Pisa*

***Submitted** to *Review of Scientific Instruments*

[†]Corresponding author, e-mail: losurdo@pi.infn.it

[‡]Now at INFN Pisa

[§]Now at ESO, Garching, Germany.

^{**}Now at University of Padova and INFN - Sez. di Padova.

^{††}Now at Caltech, Pasadena, California.

Abstract

interferometric gravitational wave detectors must be isolated from seismic noise. The VIRGO vibration isolator, called *superattenuator*, is fully effective at frequencies above 4 Hz. Nevertheless, the residual motion of the mirror at the mechanical resonant frequencies of the system are too large for the interferometer locking system and must be damped. A multidimensional feedback system, using inertial sensors and digital processing, has been designed for this purpose. An experimental procedure for determining the feedback control of the system has been defined. In this paper a full description of the system is given and experimental results are presented.

1. Introduction

The sensitivity of interferometric antennas for gravitational wave detection¹⁻⁵ is limited at low frequencies by seismic noise. In order to suppress seismic noise below the thermal noise level above 4 Hz, a special vibration isolator has been designed to suspend the mirrors of the VIRGO detector: the superattenuator (SA)⁶. The expected residual motion of the mirror is $\sim 10^{-18}$ m/ $\sqrt{\text{Hz}}$ @4 Hz. At lower frequencies, the residual motion of the mirror is much larger (~ 0.1 mm RMS), due to the normal modes of the SA (the resonant frequencies of the system are in the range 0.04-2 Hz).

In order to maintain the VIRGO interferometer locked¹⁰ the RMS motion of the suspended mirrors must not exceed 10^{-12} m. The VIRGO locking strategy is based on a hierarchical control. Feedback forces can be exerted on three points of the SA: the inverted pendulum (IP)⁷ suspension point, the marionette (a stage properly designed to steer the mirror⁸) and the mirror itself, by means of a seismic noise free recoil mass. The control on the three points is operated in different ranges of frequency and amplitude. The maximum mirror displacement that can be controlled from the marionette without injecting noise in the detection band is ~ 10 μm . Moreover, the lower the residual mirror motion the shorter the time needed for the interferometer locking. Therefore, damping of the SA normal modes is required for a correct operation of the locking system. A wideband high gain active control of the SA normal modes using sensors and actuators on top of the IP and capable of reducing the mirror residual motion within a few microns has been successfully implemented. It has been defined *inertial damping* since it mostly makes use of accelerometers.

Several previous works have been done in this field. The use of accelerometers for vibration isolation in gravitational wave experiments had already been proposed many years ago (see ref.¹² and ref. therein). More recently a multistage active vibration isolation system using multidimensional active controls has been proposed for the LIGO detector^{15,16}.

2. Experimental setup

The experimental setup (fig. 1) consists of a full scale SA, provided with three accelerometers (placed on the top of the IP), three LVDT position sensors (measuring the relative motion of the IP with respect to an external frame) and three coil-magnet actuators. The sensors and actuators are all placed in a pin-wheel configuration. The sensors and actuators signals are processed by a computer controlled ADC (16 bit)-DSP-DAC (20 bit) system. The DSP handles the signals of all the sensors and actuators, recombines them by means of matrices, creates complex feedback filters with high precision pole/zero placements and performs calculations at a high sampling rate (10 kHz).

In the following we briefly describe the main features of the digital electronics designed for the VIRGO active controls:

- **DSP:** the Virgo control system runs at 10 kHz, in order not to have excessive phase rotation at frequencies of interest (we foresee controlling the suspended masses of the interferometer up to 100 Hz). With a sampling frequency of 10 kHz, the input to output delay of our DSP system (taking into account the delay introduced by the anti-aliasing filter in front of the ADC and the corresponding low pass filter after the DAC) is about 540 μsec . This delay will introduce a phase rotation of about 20 degrees at 100 Hz, low enough for our purposes. On the other hand the system must be able to deal with very low frequencies (the main resonance of the inverted pendulum is about 40 mHz) and this requires a very high arithmetic precision in the DSP system: it can be shown that, for a second order filter, the minimum frequency that can be implemented is proportional to the square root of the arithmetic precision. For instance, the minimum frequency for a filter with a quality factor of 10 (at a sampling frequency of 10 kHz) is about 2.5 Hz with a mantissa of 24 bits, whereas it is about 0.15 Hz with a mantissa of 32 bits. The chosen processor was the DSP 96002 from Motorola, that supported the extended arithmetic precision (32 bits of mantissa) needed for our purposes.

- **ADC:** two sources contribute to the noise of an analog to digital converter: the electronic noise and the quantization noise due to the limited number of bits of the converter. The ADC is a 16 bit system with an input range of ± 10 Volt; the first noise source slightly dominates the second so that our ADC is equivalent to an ideal 15 bit ADC. The RMS value of the total noise is about $170 \mu V$; its power spectral density is uniformly distributed on the Nyquist band. At a sampling frequency of 10 kHz this corresponds to a spectral density of about $2.4 \mu V/\sqrt{\text{Hz}}$. In order to lower the noise level it is necessary to increase the sampling frequency. Our ADC is able to sample the input signal up to 200 kHz and to send to the DSP the sum of the last N samples, where N ranges from 1 to 256. Working with the ADC at 200 kHz and N equal to 20, we get a noise level of about $500 \text{ nV}/\sqrt{\text{Hz}}$. This corresponds to a dynamic range of about $143 \text{ dB}\cdot\sqrt{\text{Hz}}$ (we define the dynamic range of a system as the ratio between the maximum RMS value the system is able to manage and the spectral density noise level).
- **DAC:** our DAC system is based on an audio 20 bit converter: its measured noise level is less than $250 \text{ nV}/\sqrt{\text{Hz}}$.

The dynamic range of our digital system is almost equivalent to that of a good analog one and can be further improved by using pre-emphasis and de-emphasis filters. In addition a digital system is much more flexible for what concerns the complexity of the filters that can be implemented, the precision and the time stability of the filter parameters.

3. From a MIMO to a SISO system

The IP is a three degrees of freedom mechanical system: three independent sensors are required to fully determine its position and three independent actuators to move the IP in the required settings. The sensors and the actuators are mounted on the top stage in triangular configuration. Each sensor is, in principle, sensitive to movements in all the three

IP normal modes (which are defined as x, y, θ , although they do not correspond necessarily to pure translations and rotations). In the same way, each actuator will generate movements of the IP involving a mix of the three modes. The basic idea of the IP controls, which applies both to the inertial damping and the position control, is to *diagonalise* the sensing and control actions: the aim is to pass from the sensor/actuator space, to a space where each normal mode is independently sensed and acted upon. Mathematically, this means to realize a coordinate transformation such that the equations of motion have the form:

$$\ddot{x}_i + \omega_i^2 x_i = q_i \tag{1}$$

where the x_i (for $i = 1, 2, 3$) is a normal coordinate, $\omega_i/2\pi$ is the resonant frequency of the i -th mode and q_i is the generalized force corresponding to the coordinate x_i ¹⁴. This means to find three linear combinations of the sensor outputs, defined *virtual sensors*, each sensitive to a single normal mode and, correspondingly, three linear combinations of the excitation coil currents (*virtual actuators*) which excite each mode separately. In control theory terminology, this means to break down a *multiple in-multiple out* (MIMO) system into many *single in-single out* (SISO) systems. The control of a SISO system is much easier: every mode is controlled by an independent feedback loop, simplifying greatly the loop design and the stability requirements. In this chapter we describe a possible approach to the problem. A more general approach would require the system description in the state space representation (see for instance ref.^{11,13}).

4. Diagonalization: the parameter search scheme.

Several approaches to the diagonalisation problem have been defined. In this paper we describe the fastest one. Other procedures are described in ref.^{9,13}.

In the parameter search scheme the sensor/driver/mechanical-response system is described by a set of parameters. Sets of excitation/response data are taken and stored on disk. A merit function is constructed that is related to the degree of success of diagonalization. The space of system parameters is then searched using standard algorithms in order

to maximize the merit function.

A. Merit Function

If the resonance peaks are well separated from each other the value of the imaginary part of the transfer function of an arbitrary, 'real', sensor shows two distinct peaks in the region of the IP translational modes. A diagonalized, 'virtual', sensor should show only one peak. We construct a merit function by integrating the (absolute) value under the two peaks. If the diagonalization is correct, then there should be only a small amount of y -mode in the x -peak and vice versa. In addition, the amount of the rotational mode present in the x and y peaks should be small. The merit function is constructed using a weighted sum of appropriate ratios of these integrated values.

This merit function is then used with a MATLAB routine FMINSEARCH and the parameters are varied to find the best result. The sensing matrix obtained by this so-called 'automatic' diagonalization agrees well with that obtained by other procedures. We illustrate this by showing some data taken from the injection bench suspension tower. In fig. 2 the response of *real* and *virtual* sensors is compared.

In the case where the two IP translational peaks are degenerate, or almost degenerate, there are two alternative paths. One is to declare victory and say that if the modes are degenerate any two orthogonal directions are as good as any other; then choose the most convenient set. The other path is to do the best you can and then look at the very low frequency part of the LVDT spectra and the accelerometer spectra above several Hertz where most of the resonance activity is absent. Simple average values in these regions can be used as merit functions. A check on the reliability of the results is that the diagonalized modes of the LVDT's, the accelerometers, and the coil drivers should be approximately related to each other by known rotations.

B. Selection of the Parameter Set

The ultimate goal in the diagonalization process is to find a sensing matrix that transforms sensor outputs into $x-y-\theta$ displacement values and to find a driving matrix that transforms desired $x-y-\theta$ displacements into driver-coil currents (see fig. 3). The chosen parameter set should make this task as simple as possible and should have a clear association with the component systems.

Certain parameters are fixed and known: the positions and orientations of the sensors and coils. Other parameters such as the relative sensitivity of the sensor and drive-coil components should be within a few percent of unity. Finally, if there is no mixing between the two translational modes and the rotational mode, there is only one parameter that we have no a priori knowledge: the angle ψ between the translational mode coordinate system and the laboratory system. We start our discussion with the simplest case; all system component sensitivities are the same and, also, there is no mode mixing. We will add these complications later.

The components of the horizontal LVDT's, accelerometers and coil driver systems are arranged in groups of three, positioned 120 degrees apart with respect to each other. We denote a system state by a vector $s = [a \ b \ c]$, the values of the three components. A translation and/or rotation of the IP results in signals in the sensor components given by

$$s = \begin{pmatrix} a \\ b \\ c \end{pmatrix} = \mathbf{D} \begin{pmatrix} u \\ v \\ r \theta \end{pmatrix}$$

Here, u and v are translations, θ is a rotation and r is the radius of the sensor system. The 3×3 matrix \mathbf{D} contains the geometry of the sensor system. For example given a set of 3 sensors at respective $u-v$ angles of ϕ , $\phi + 120$ and $\phi + 240$ degrees: the \mathbf{D} matrix is:

$$\mathbf{D} = \begin{bmatrix} \sin(\phi) & \cos(\phi) & 1 \\ \sin(\phi + 2\pi/3) & \cos(\phi + 2\pi/3) & 1 \\ \sin(\phi + 4\pi/3) & \cos(\phi + 4\pi/3) & 1 \end{bmatrix}$$

The relative gain of the sensors can be easily incorporated at this point by letting \mathbf{D} be multiplied by a 3×3 diagonal gain matrix: $\mathbf{D} \implies \mathbf{G} \mathbf{D}$

A 3-vector s describing the state of one of the system can be transformed back into its equivalent spatial representation; a $u - v$ translational vector plus a rotation. This is obtained by multiplying the state vector by a 3×3 matrix, \mathbf{R} :

$$\begin{pmatrix} u \\ v \\ r \theta \end{pmatrix} = \mathbf{R} \begin{pmatrix} a \\ b \\ c \end{pmatrix} \quad \text{where } \mathbf{R} = \mathbf{D}^{-1}$$

Thus, for example, given $\phi = 0$, \mathbf{D} and \mathbf{R} become

$$\mathbf{D} = \begin{bmatrix} 0 & 1 & 1 \\ -0.866 & -0.5 & 1 \\ 0.866 & -0.5 & 1 \end{bmatrix} \quad \mathbf{R} = \begin{bmatrix} 0 & -0.577 & 0.577 \\ 0.667 & -0.333 & -0.333 \\ 1/3 & 1/3 & 1/3 \end{bmatrix}$$

Multiplying the first two rows of \mathbf{R} by the scaling factor $\sqrt{3}/2$ and the last row by $\sqrt{3}$ we obtain the 'standard' sensing matrix (where each line is normalized to 1):

$$\mathbf{S} = \begin{bmatrix} 0 & -0.707 & 0.707 \\ 0.817 & -0.408 & -0.408 \\ 0.577 & 0.577 & 0.577 \end{bmatrix}$$

The sensing matrix \mathbf{S} happens to be an orthogonal matrix corresponding to a rotation in three dimensions. This rotation can be constructed by choosing three Euler angles according to the following prescription:

1. Rotate an amount $\theta = 45^\circ$ clockwise about the z -axis.

2. Rotate an amount $\phi = \cos^{-1}(1/\sqrt{3}) = 54.7^\circ$ clockwise about the y' -axis.
3. Rotate an amount $\psi = 210 - \phi_0$ clockwise about the the z'' axis. Here, ϕ_0 is the angle of the sensor system.

We note that the values for θ and ϕ do not depend on the angle of the sensor system nor on the direction of the $x - y$ axes. Thus for this most *simple case*, equal component gains and no mode mixing, a sensing matrix can be constructed by finding the correct relative angle between the sensor system and the $x - y$ axes. A scan in the variable ψ is all that is needed.

Complications

The case where the sensor components have different relative gain has been discussed; we multiply \mathbf{D} by a diagonal gain matrix which gives $\mathbf{D} \implies \mathbf{G} \mathbf{D}$ and $\mathbf{S} \implies \mathbf{D}^{-1} \mathbf{G}^{-1}$.

If the relative angles of the sensor components are not exactly 120° apart the resulting \mathbf{S} matrix can no longer be described by an orthogonal rotation but must be slightly modified. Suppose, for example, in the relation $s = (a \ b \ c) = \mathbf{D}(x \ y \ r\theta)$ the element corresponding to a is rotated by a small angle γ . Then a new vector

$$s' = \begin{pmatrix} a' \\ b \\ c \end{pmatrix} = \mathbf{A} \begin{pmatrix} a \\ b \\ c \end{pmatrix} = \begin{bmatrix} \alpha & \beta & -\beta \\ 0 & 1 & 0 \\ 0 & 0 & 1 \end{bmatrix} \begin{pmatrix} a \\ b \\ c \end{pmatrix}$$

can be defined with $\alpha = \cos(\gamma)$ and $\beta = \sin(\gamma)/\sqrt{3}$. The modified sensing matrix becomes $\mathbf{S} \implies \mathbf{D}^{-1} \mathbf{A}^{-1}$. The effect is not large, a misalignment of 10 mrad mixes the components by one percent or so.

In summary we have identified five parameters to define the sensing matrix; one angle ψ , two relative sensor gains, g_2/g_1 , g_3/g_1 , and two misalignment angles γ and ρ . This parameter space is then searched to maximize the merit function. In practice, we have found that it is sufficient to vary the single parameter ψ to obtain a set of diagonalization parameters enabling us to close the inertial damping feedback loops. Fig. 4 shows the effect of the diagonalization on the SA transfer function.

5. Inertial damping: principle

The control we describe here is called *inertial damping* because it is performed by using (mostly) *inertial sensors* (accelerometers). In the following, with the help of a simple model, we explain why this is the best choice to achieve a high performance damping.

Let us consider a simple pendulum of mass m and length l . Let x be the abscissa of the suspended mass, x_0 that of the suspension point. Let F_{fb} the external force on the pendulum (i.e. the feedback force to control it). The equation of motion is then:

$$F_{\text{fb}} = m\ddot{x} + \gamma\dot{x} + k(x - x_0) \quad (2)$$

where γ is the viscous dissipation factor and $k = mg/l$. The control loop of such a system is sketched in fig. 5, where $H(s)$ is the mechanical transfer function, $G(s)$ is the compensator and out is the output of the sensor used. The goal of the control is the damping of the pendulum resonance. This can be done easily with a *viscous* (theoretical) feedback force:

$$F_{\text{fb}} = -\gamma'\dot{x} \quad (3)$$

Our sensors do not measure x . Their output is:

$$out = \begin{cases} x - x_0 & \text{for displacement sensors} \\ \ddot{x} & \text{for accelerometers} \end{cases} \quad (4)$$

Therefore, the actual “viscous” force that can be built if position sensors are used has the form:

$$F_{\text{fb}}^p = -\gamma' \frac{d}{dt}(x - x_0) \quad (5)$$

It can be easily shown that with such a feedback force the closed loop equation of motion (in Laplace space) reduces to:

$$x(s) = \frac{\omega_0^2 + G_0 s}{s^2 + \omega_0^2 + (\omega_0/Q + G_0)s} \cdot x_0(s) \quad (6)$$

where $G_0 = \gamma'/m$ is a gain parameter (in a real feedback system a frequency dependent gain function $G(s)$ rather than a fixed gain parameter has to be considered) measuring the

intensity of the viscous feedback force, and Q is the open loop quality factor. When the loop is closed a damping of the resonance is achieved:

$$Q' \xrightarrow{G \gg 1} \frac{\omega_0}{G} \quad (7)$$

Nevertheless, as the gain is increased, a larger amount of noise is reinjected off-resonance. This is associated to the term “ G_0s ” in the numerator of (6) and depends on the fact that the sensor used to build up the feedback force measures the position of the pendulum with respect to ground. Therefore, an infinitely efficient feedback would “freeze” the pendulum to ground (which is seismic noisy), reducing its motion at the resonance, with the drawback of bypassing its attenuation properties above resonance.

The situation is fairly different when an inertial sensor is used. In this case the viscous feedback force is obtained by integrating the accelerometer output, which does not depend on x_0 :

$$F_{\text{fb}}^a = -\gamma' \int \ddot{x} dt \quad (8)$$

The closed loop equation of motion is then:

$$x(s) = \frac{\omega_0^2}{s^2 + \omega_0^2 + (\omega_0/Q + G_0)s} \cdot x_0(s) \quad (9)$$

A damping of the resonance is obtained (exactly as in the previous case) but without reinjection of off-resonance noise. In fig. 6 a simulation of the closed loop transfer function $x(s)/x_0(s)$ is shown in the two cases.

Up to now we have considered a simple viscous damping. It is possible to increase the bandwidth of the control if the feedback force contains a term proportional to x (the double integral of the accelerometer signal). The result obtained in this case is shown in fig. 7.

6. Control strategy

In this section we extend the principles of the previous section and describe the strategy to control the SA.

The basic idea of inertial damping is to use the accelerometer signal to build up the feedback force. As a matter of fact a perfect feedback using only the inertial sensor information would null the acceleration of the pendulum but it would do nothing if the pendulum moved at constant velocity: such a control is unstable with respect to drifts. Therefore, if the control band is to be extended down to DC, a position signal is necessary. Our solution is to merge the two sensors: the virtual LVDT (position) and accelerometer signals are combined in such a way that the LVDT signal ($l(s)$) dominates below a chosen crossover frequency f_{merge} while the accelerometer signal ($a(s)$) dominates above it (see fig. 8). The feedback force has the form :

$$F_{\text{fb}} = G(s) [a(s) + \epsilon l(s)] \quad (10)$$

where $G(s)$ is the transfer function of the compensator and ϵ is the parameter whose value determines f_{merge} . We choose $f_{\text{merge}} \sim 10$ mHz (corresponding to $\epsilon \sim 5 \cdot 10^{-3}$). This approach stabilizes the system with respect to low frequency drifts at the cost of reinjecting a fraction ϵ of the seismic noise via the feedback. In order to reduce the amount of reinjected noise at $f > f_{\text{merge}}$ (while preserving feedback stability at the crossover frequency) the LVDT signal $l(s)$ is properly low-pass filtered.

We describe in the following the feedback design for the three d.o.f., starting from the translational ones. The virtual X and Y sensors show many resonant peaks (the modes of a chain of pendulums) and this requires a more sophisticated feedback strategy. The digital filter used to control the translation modes ($G(s)$) is shown in fig. 9 (LEFT). It shows three main features:

- for $0.01 < f < 2$ Hz the gain is proportional to f^{-2} . This corresponds to the case of fig. 7: the accelerometer signal is integrated twice and the feedback force is proportional to x ;
- for $f > 2$ Hz the gain is proportional to f^{-1} . The accelerometer signal is integrated once: the feedback force is proportional to the velocity and a viscous damping is achieved;

- the peaks visible in the filter are necessary to compensate the corresponding dips in the mechanical transfer function ($H(s)$) of fig. 4, in order to make the feedback stable.

Fig. 9 (RIGHT) shows the open loop gain transfer function $G(s)H(s)$.

The damping strategy for the Θ mode is simpler: the Θ virtual sensor shows one resonance peak only and no dips (see fig. 4, RIGHT): no compensation is necessary. Apart from this, the feedback strategy is similar to the ones used for the translational modes.

7. Inertial damping: experimental results

Results of the inertial control (on three d.o.f.) are shown in figure 10. This measurement was performed in air on the prototype SA. The noise at the top of the IP is reduced over a wide band (10 mHz - 4 Hz). A gain greater than 1000 was obtained at the main SA resonance (0.3 Hz). The RMS translational motion of the IP (calculated as $x_{\text{RMS}}(f) = \sqrt{\int_f^\infty \tilde{x}^2(\nu) d\nu}$) in 10 sec. is reduced from more than 30 to 0.3 μm . The closed loop floor noise corresponds to the fraction of seismic noise reinjected by using the position sensors for the DC control and can, in principle, be reduced by a steeper low pass filtering of the LVDT signal at $f > f_{\text{merge}}$ and by lowering f_{merge} : both this solutions have drawbacks and require careful implementation.

The control strategy adopted in this experiment requires a careful compensation of the dips in the transfer function. A less aggressive strategy has been adopted for the SA on VIRGO site. The filter is a simple integrator (plus compensation of high frequency structural resonance). The gain is lower but no compensation of the dips is needed. This makes the control loops more robust with respect to changes of the frequency of the poles and zeroes in the transfer function that might be induced by temperature variations. Results (obtained under vacuum, on the VIRGO site) are shown in fig. 11 for the 3 d.o.f.. Even if the gain of the loop is less in this case, the measured closed loop noise floor is lower because the system is under vacuum.

Inertial damping is a technique for damping the normal modes of the VIRGO suspension and reducing seismic noise entering the system. The measurements presented in this paper

demonstrate the success of the method. Further measurements of the mirror motion with and without inertial damping are necessary to prove directly the reduction of the residual mirror motion. These measurements will be the topic of a forthcoming paper.

REFERENCES

1. A.Abramovici, *et al.*, *Science*, **256**, 325 (1992).
2. C.Bradaschia, *et al.*, *Nucl. Instrum. Meth. A*, **289**, 518 (1992).
3. J.Hough, K.Danzmann, *et al.*, *GEO600 Proposal*, unpublished (1994).
4. K.Kuroda, *et al.*, in *Proceedings of the 1st International Conference on GW: Sources and Detectors*, eds. F.Fidecaro, I.Ciufolini, World Scientific, Singapore (1997).
5. D.McClelland, D.G.Blair, R.J.Sandeman, *AIGO: A Southern Hemisphere Second Generation Gravitational Wave Observatory*, in *Proceedings of the 7th Marcel Grossmann Meeting on General Relativity*, Part B, (Stanford Univ. July 1994), Eds: R.T. Jantzen, G.M. Keiser, Series ed. R. Ruffini, World Scientific Pub.Co, 1415-1417 (1996).
6. G.Ballardin, *et al.*, *Measurement of the VIRGO Superattenuator performance*, accepted for publication by *Rev. Sci. Instrum.* (2001).
7. G.Losurdo, *et al.*, *Rev. Sci. Instrum.*, **70** (5), 2507-2515 (1999).
8. A.Bernardini, E.Majorana, P.Puppo, P.Rapagnani, F.Ricci, G.Testi, *Rev. Sci. Instr.*, **70** (8), 3463 (1999).
9. G.Losurdo, PhD thesis, Scuola Normale Superiore, Pisa (1998).
<http://www.virgo.infn.it/Documents/ftpvirgo/Archive/Thesis/DottLosurdo.ps>
10. R.Flamini, H.Heitmann, *Phys. Lett. A*, **214**, 112 (1996).
11. K.Ogata, *Modern control engineering*, Prentice-Hall International (1997).
12. P.R.Saulson, *Rev. Sci. Instr.*, **55**, 1315 (1984).
13. A.Gennai, S.Mancini, T.Maiani, D.Passuello, VIRGO internal report, VIR-NOT-PIS-1390-101 (1997).
14. H.Goldstein, *Classical Mechanics*, Addison-Wesley, Reading (1980).

15. S.J.Richman, J.A.Giaime, D.B.Newell, R.T.Stebbins, P.L.Bender, J.E.Faller, *Rev. Sci. Instrum.*, **69** (6), 2531 (1998).
16. J.Giaime, *et al.*, LIGO internal report, LIGO-E010016-00-D (2001).
<http://www.ligo.caltech.edu/docs/E/E010016-00.pdf>
17. G.Losurdo, *Inertial control of the VIRGO superattenuator*, in *Proceedings of the Third E.Amaldi Conference on gravitational waves experiments*, Pasadena, 12-16 July 1999, editor S.Meshkov, World Scientific (2000). Also gr-qc/9911044.

FIGURES

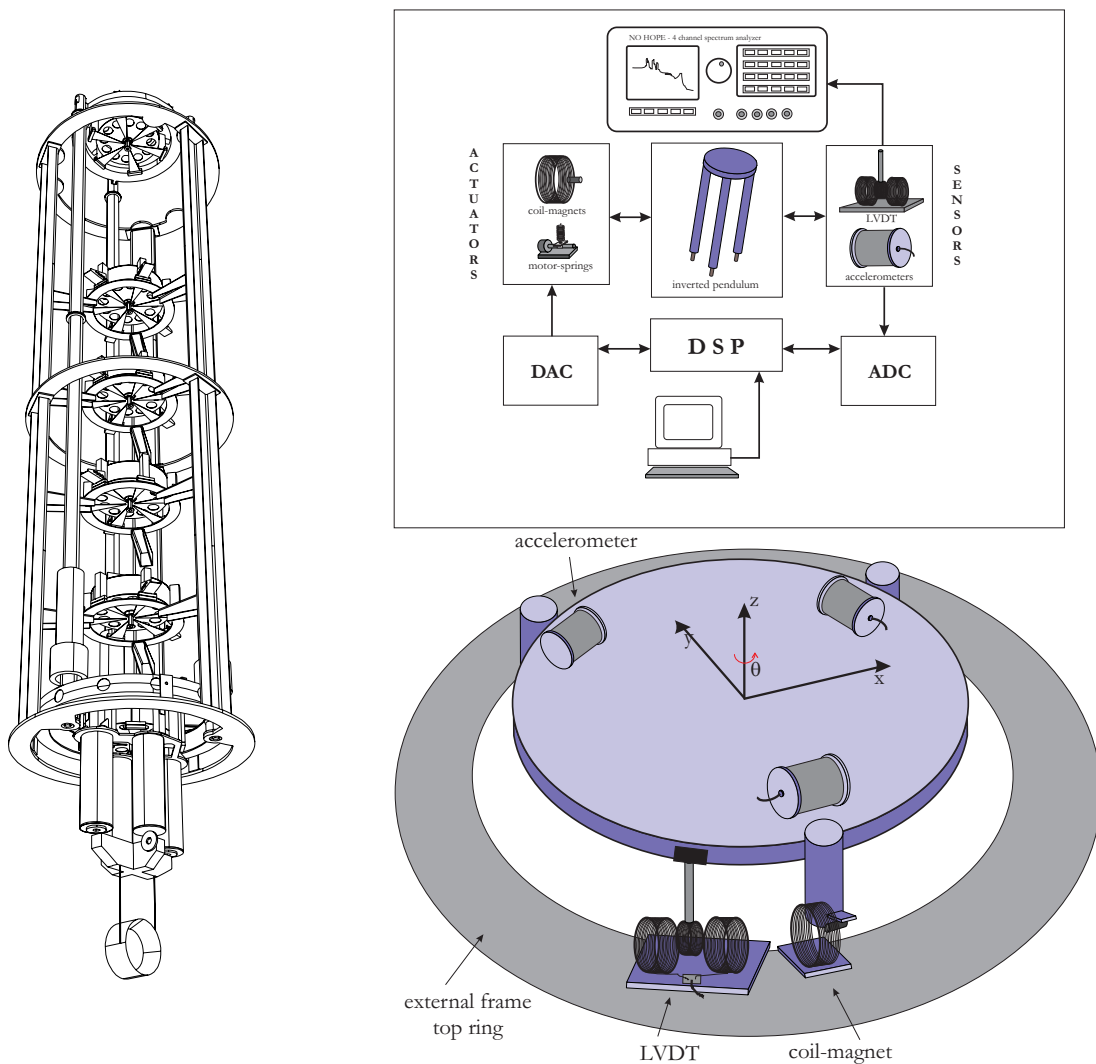


Fig. 1. LEFT: the superattenuator; RIGHT TOP: logical scheme of the setup for the local active control; RIGHT BOTTOM: simplified view of the IP top table, provided with the 3 accelerometers. One LVDT position sensors and one coil-magnet actuator are also shown.

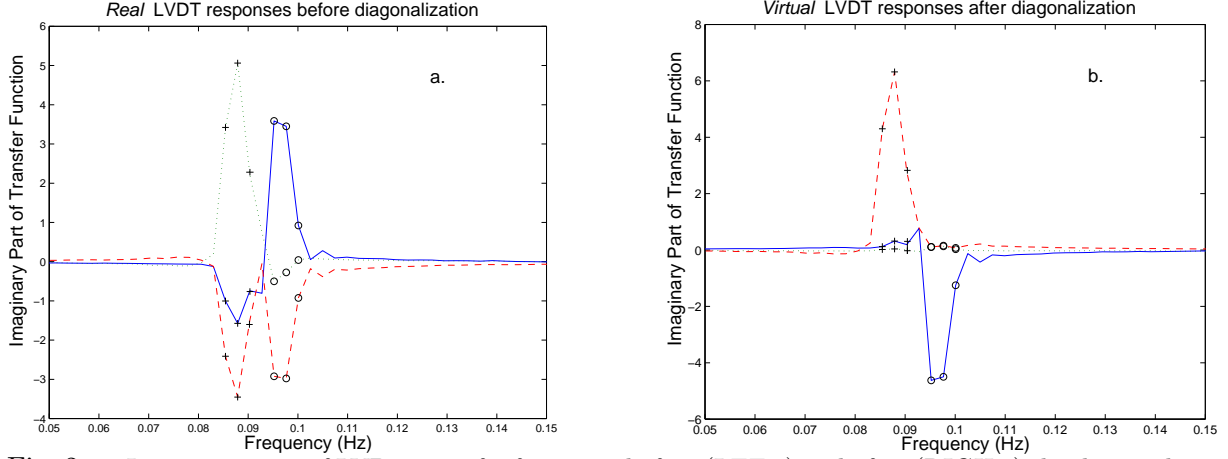


Fig. 2. Imaginary part of LVDT transfer functions before (LEFT) and after (RIGHT) the diagonalization procedure. The + and o marks correspond to the integration points for the X and Y translation modes respectively. The solid, dashed, and dotted curves in (LEFT) correspond to the 'real' LVDTs whereas in (RIGHT) they correspond to the X , Y and rotational combinations. Only one of the three coils was energized for this data set.

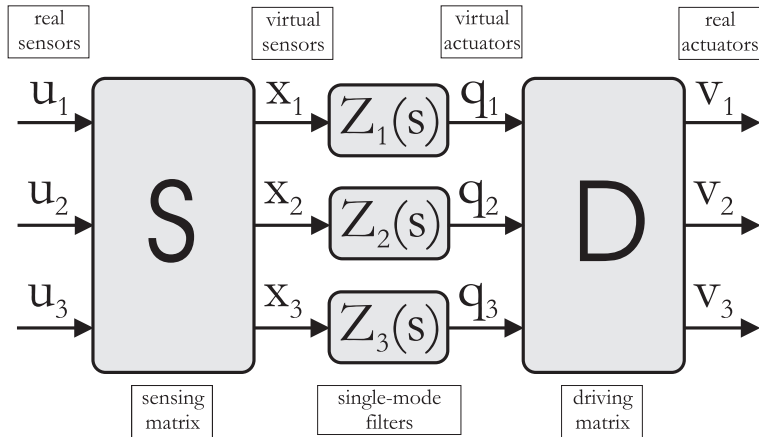


Fig. 3. Decomposition of a 3-modes system into 3 non-interacting 1-mode systems: the real sensors signals x_i are recombined by the matrix S to create the virtual sensors x_i . Each virtual sensor is acted upon independently. The virtual forces q_i are defined by the filters z_i . The virtual forces are converted into voltages driving the real actuators by the matrix D .

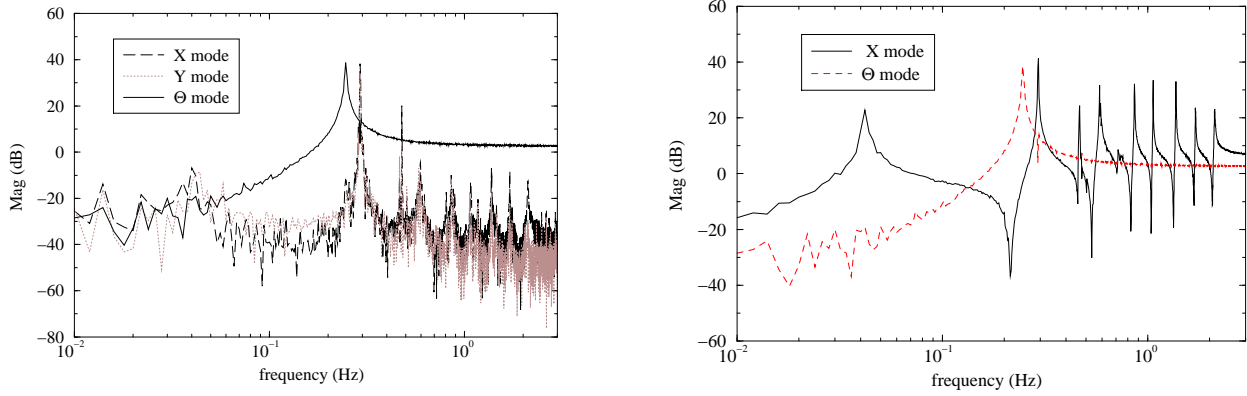


Fig. 4. Effect of the digital diagonalisation. LEFT: the output of the 3 virtual accelerometers when Θ is excited. RIGHT: the output of the virtual accelerometers X and Θ are compared. Different feedback strategies are required in the two cases, because X senses all the translational modes of the SA chain.

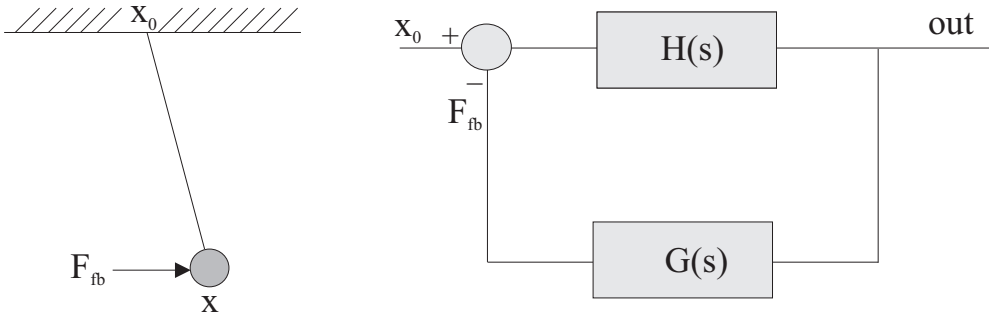


Fig. 5. The control scheme for a simple pendulum: $H(s)$ is the mechanical transfer function, $G(s)$ the compensator filter.

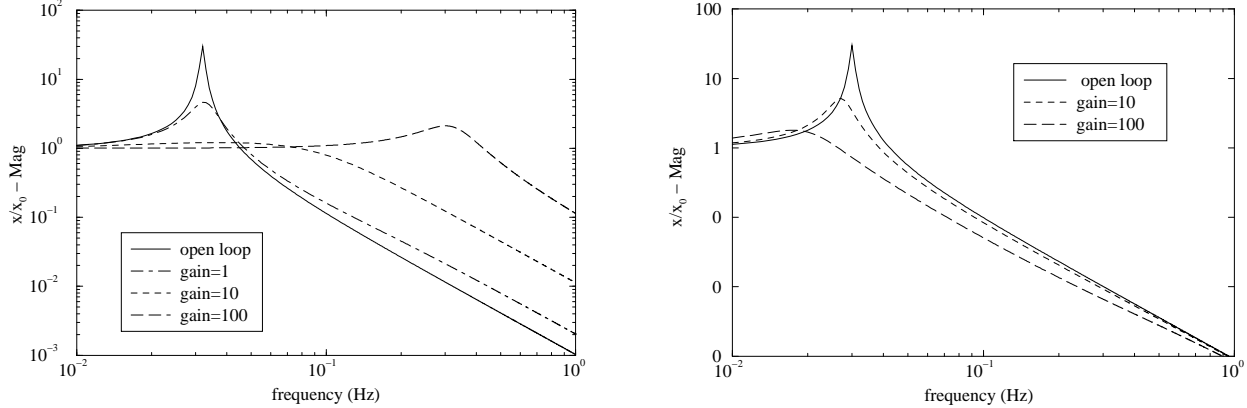


Fig. 6. Damping of a simple pendulum: the closed loop transfer function $x(s)/x_0(s)$ (magnitude) when a position sensor is used (LEFT) and when an accelerometer is used (RIGHT). In the first case it is evident the re-injection of noise above the resonance.

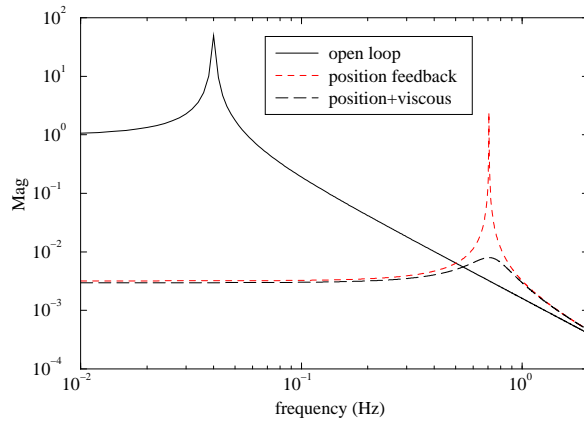


Fig. 7. Inertial damping of a simple pendulum when a position feedback is implemented.

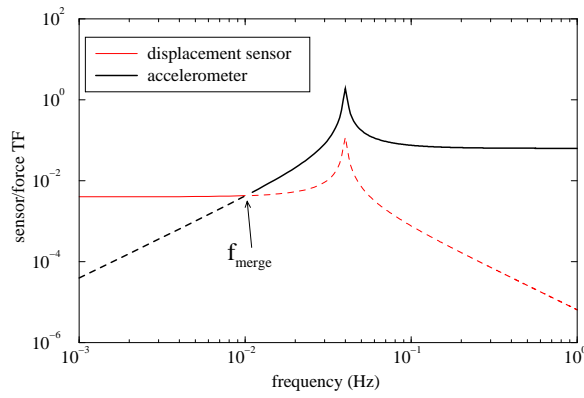


Fig. 8. *Merging* of displacement and acceleration sensors (simulation for a simple pendulum).

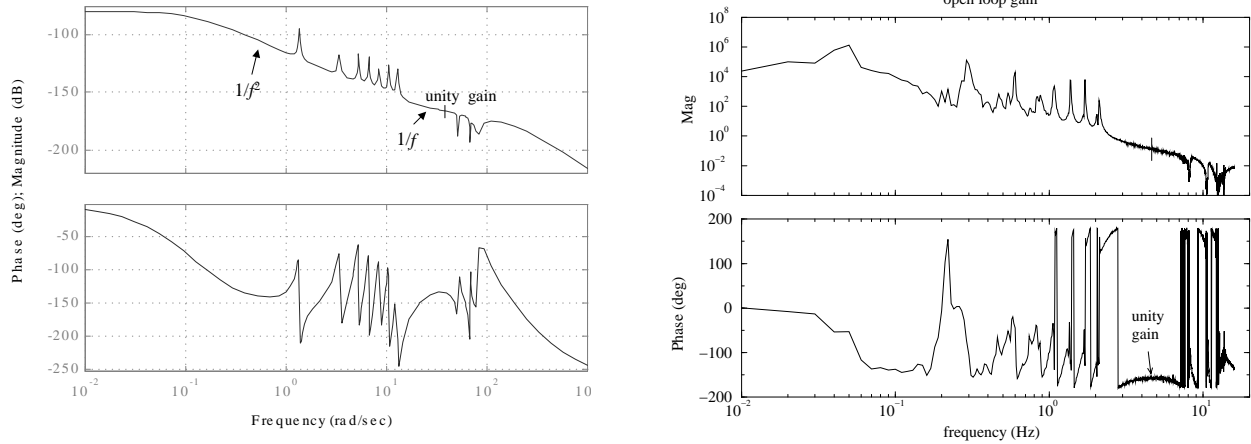


Fig. 9. LEFT: Digital filter used for the inertial damping of a translation mode (X). The filter slope is f^{-2} in the range $10 \text{ mHz} < f < 3 \text{ Hz}$, f^{-1} for $f > 3 \text{ Hz}$. The unity gain is at 4 Hz. The peaks in the digital filter are necessary to compensate the dips in the mechanical transfer function (see the transfer function of the X mode in fig. 4). RIGHT: open loop gain function (measured). The phase margin at the unity gain frequency is about 25° .

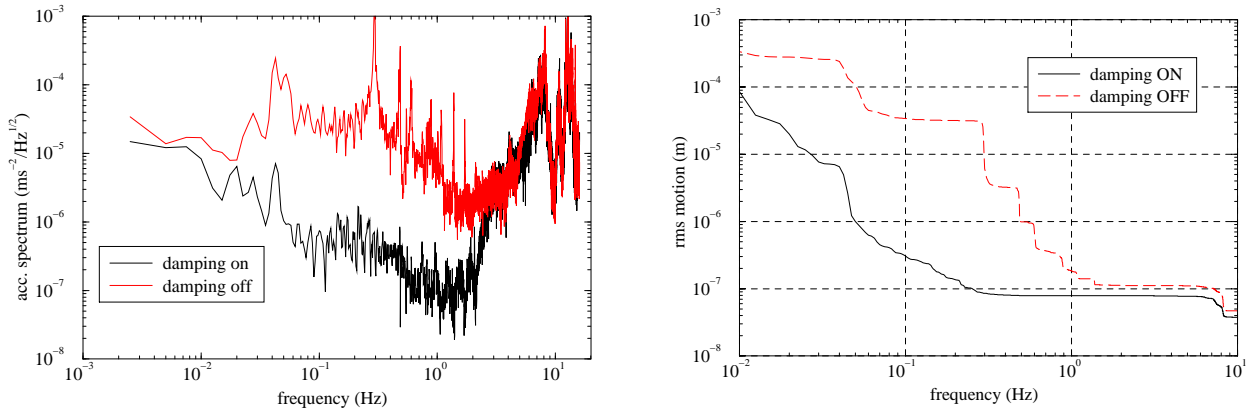


Fig. 10. Performance of the inertial control (X, Y, Θ loops closed) of the superattenuator, measured on the top of the IP: the left plot shows the acceleration spectral density as measured by the *virtual* accelerometer X (translation). The right plot shows the effect of the feedback on the RMS residual motion of the IP as a function of the frequency.

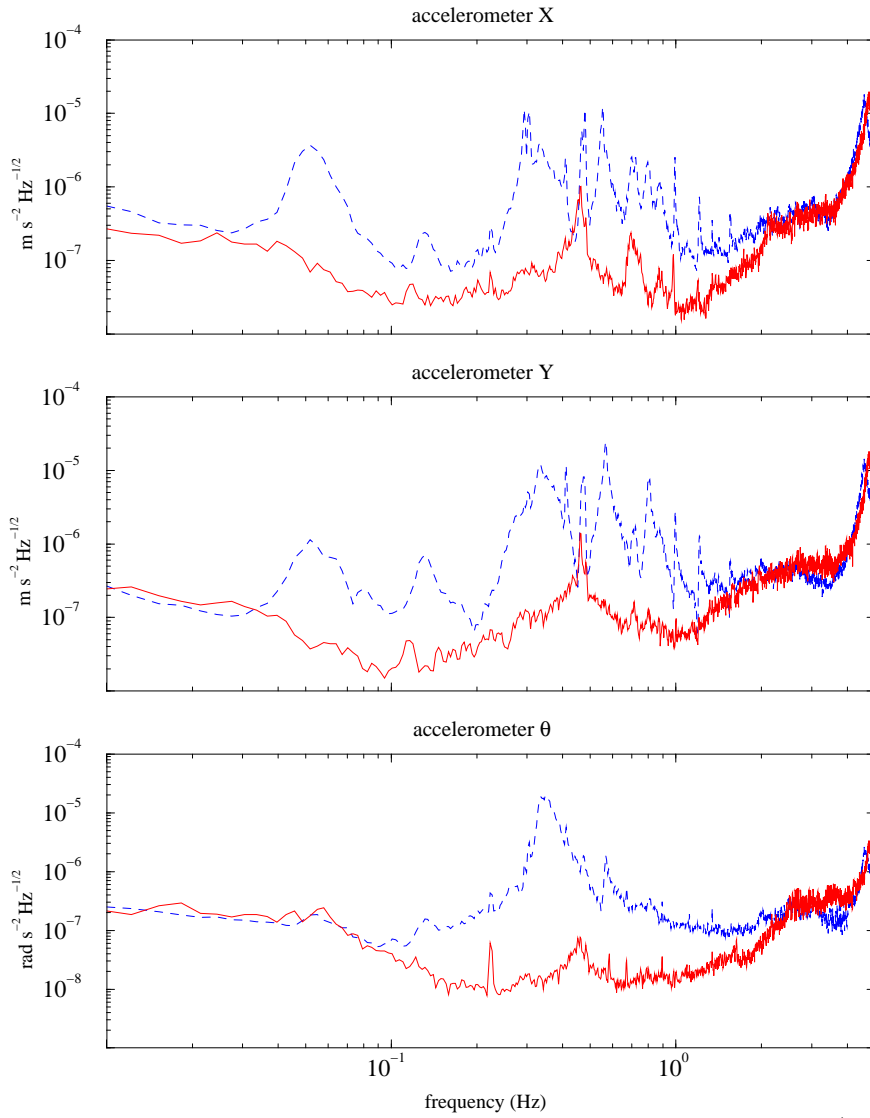


Fig. 11. Performance of the inertial damping on one of the VIRGO superattenuators (the 3 d.o.f. Θ , Y , X are shown, the system was under vacuum).